Emergence of Spontaneous Twist and Curvature in Non-Euclidean Rods: Application to *Erodium* Plant Cells

Hillel Aharoni,[1] Yael Abraham,[2] Rivka Elbaum,[2] Eran Sharon,[1] and Raz Kupferman[3]

[1]*Racah Institute of Physics, The Hebrew University of Jerusalem, Jerusalem 91904, Israel*
[2]*Robert H. Smith Institute of Plant Sciences and Genetics in Agriculture, The Hebrew University of Jerusalem, Rehovot 76100, Israel*
[3]*Institute of Mathematics, The Hebrew University of Jerusalem, Jerusalem 91904, Israel*

We present a limiting model for thin non-Euclidean elastic rods. Originating from the three-dimensional (3D) reference metric of the rod, which is determined by its internal material structure, we derive a 1D reduced rod theory. Specifically, we show how the spontaneous twist and curvature of a rod emerge from the reference metric derivatives. Thus, the model allows calculating the unconstrained equilibrium configuration of a thin rod directly from its internal structure. The model is applied to the study of cells from members of the *Geraniaceae* plant family and their configurational response to dehydration. We show how the geometrical arrangement of cellulose fibrils on the cell walls determines the helical shapes of isolated cells.

Plant tissues commonly exhibit humidity-induced conformational changes that fulfill functional roles, such as the control of seed dispersal. Examples of such mechanisms are found in pine cones [1] and in seed pods [2] or awns [3]. In these cases, the plant tissue that is responsible for seed dispersal is sclerenchymal; the cells have thick walls which cause a strictly mechanical reaction to stress. Humidity changes cause the tissue to absorb (expel) water and therefore swell (shrink) nonuniformly. Elastic stresses that form as a result of differential changes in volume may partially relax via changes in the conformation of the organ. Mechanical models that explain conformational changes in sphere- [4], plate- [5], and shell- [6,7] like organs have been studied, linking the local swelling (shrinkage) of the tissue to the global shape changes of the organ.

Another common structure in nature is thin rodlike organs. Rodlike structures in plants include tendrils [8], awns [3], or even individual cells [9,10]. Such structures undergo extremely large shape transformations in response to growth or external stimuli. In [10], for example, it was demonstrated how a flexible tissue wrapped with an inextensible fiber twists as a response to volume change. More general mechanical models of rodlike organs have traditionally focused on obtaining their shape [8] and dynamics [11], given an *intrinsic curvature* and an *intrinsic twist*. However, no connection has been established between such intrinsic geometric parameters and the microstructure of the organs. At present, there is no general theory that provides links between the three-dimensional (3D) microstructure of a rodlike organ, its shrinking (swelling) field, and the resulting equilibrium configuration.

In this Letter, we use the framework of incompatible elasticity to derive such a general theory. Specifically, we provide a recipe whose ingredients are as follows. (i) Modeling the 3D geometry of elastic rodlike organs

from their microstructure, resulting in a 3D incompatible elasticity problem. (ii) Deriving from the 3D problem a 1D dimensionally reduced model. The effective model identifies at every point along the rod an intrinsic curvature and an intrinsic twist. (iii) Solving the equilibrium configuration of the 1D model to predict the conformation of the organ.

We apply our scheme to stork's bill (*Erodium gruinum*) and cranesbill (*Geranium pusillum*) cells, relying on the architecture of the cellulose fibrils building their walls. We compare our predictions with the measured shapes of these cells upon dehydration and find good quantitative agreement.

Incompatible elasticity.—Mathematically, we model an elastic body as a three-dimensional manifold, which we denote by $\mathcal{M}$. The intrinsic geometry of the body is prescribed in the form of a *metric tensor* $\bar{g}$. A configuration is an embedding $f: \mathcal{M} \to \mathbb{R}^3$ of this manifold into the physical Euclidean space. Every such embedding induces on $\mathcal{M}$ a metric g. Any discrepancy between g and $\bar{g}$ results in an elastic strain. An energy functional that determines the energetic cost of such a strain completes the description of the elastic problem. An equilibrium configuration is a minimizer of this energy functional.

Dimension reduction.—In order to study a body that is slender across m dimensions, we introduce a $(3 - m)$-dimensional submanifold $\mathcal{S} \subset \mathcal{M}$ and identify a thin body of thickness $2r$ with the subdomain Ω_r of points that are within a distance r of the submanifold $\mathcal{S}$ (where distances are measured with respect to the intrinsic metric $\bar{g}$). To each configuration, $f_r: \Omega_r \to \mathbb{R}^3$ corresponds to an elastic energy $E_r[f_r]$.

Under certain conditions, for example, when the body is unconstrained, the submanifold $\mathcal{S}$ can be isometrically embedded in $\mathbb{R}^3$. If $\mathcal{S}$ can be isometrically embedded

PHYSICAL REVIEW LETTERS

without "sharp bends" (a notion that can be made precise), the leading energy contribution is due to deviations of the thin surroundings of $\mathcal{S}$ from the stretch-free state. The energy of the equilibrium configuration then scales like $O(r^{m+2})$ and can be identified as a *bending* contribution. For this reason, the property of $\mathcal{S}$ being isometrically embeddable in $\mathbb{R}^n$ smoothly enough is referred to as a *finite bending property*. Note that the existence of a finitely bent isometry is an intrinsic property of $\mathcal{S}$ and its metric (induced by $\bar{g}$).

Under the assumption that finitely bent isometries of $\mathcal{S}$ in $\mathbb{R}^3$ exist, Kupferman and Solomon [12] proved the following.

(i) The family of equilibrium configurations f_r converges to a limit as $r \to 0$. This limit consists of an embedding $F: \mathcal{S} \to \mathbb{R}^3$ along with a mapping $\mathbf{q}$ of orientations on $\mathcal{S}$ into orientations in $\mathbb{R}^3$. The finite bending property reflects in that $\mathbf{q}$ is an orientation-preserving rotation, namely, $\mathbf{q} \in SO(3)$. Consistency requires that $\mathbf{q}^\| = dF$, where $\mathbf{q}^\|$ is the restriction of $\mathbf{q}$ to the tangent space of $\mathcal{S}$.

(ii) The limiting configuration $(F, \mathbf{q})$ is the minimizer of a limiting energy functional $E_{\lim}$, which is the Γ limit [13] of the sequence of functionals $r^{-(m+2)}E_r$. The limiting functional is

$$E_{\lim}[F, \mathbf{q}] = \frac{YV_m}{4(m+2)} \int_{\mathcal{S}} [|(\nabla \mathbf{q})^\perp|_\perp^2 + 2|(\nabla \mathbf{q})^\perp|_\|^2]\sqrt{\det \bar{g}}dx,$$

$$\tag{1}$$

where Y is the material's Young's modulus (we assume here a zero Poisson ratio), V_m is the volume of the (Euclidean) m-dimensional unit sphere, ∇ is the covariant derivative on $\mathcal{S}$, and $|\cdot|_\perp$ and $|\cdot|_\|$ represent the norms of the projections onto the subspaces perpendicular and tangent to $\mathcal{S}$.

Plates and shells correspond to the case $m = 1$, i.e., $\mathcal{S}$ is a surface and the limiting configuration F is an isometric embedding of that surface in three-dimensional space. In that case, (1) reduces to the expression for the bending energy of thin shells and plates presented in [2] (with a zero Poisson ratio).

Rods correspond to the case $m = 2$. Taking x^1 to be the axis tangent to the longitudinal axis of the rod and x^2 and x^3 be axes normal to x^1, the limiting configuration F only determines the unit vector $\mathbf{q}_1$ while the choice of normal directions $\mathbf{q}_2$ and $\mathbf{q}_3$ remains an additional degree of freedom of the limiting configuration. After simple algebraic manipulations, the limiting energy functional takes the form

$$E_{\lim}[F, \mathbf{q}] = \frac{\pi Y}{8} \int_{\mathcal{S}} [(\mathbf{q}_2' \cdot \mathbf{q}_1 - \Gamma_{12}^1)^2 + (\mathbf{q}_3' \cdot \mathbf{q}_1 - \Gamma_{13}^1)^2$$
$$+ (\mathbf{q}_3' \cdot \mathbf{q}_2 - \Gamma_{13}^2)^2]dx^1, \tag{2}$$

where primes denote derivatives with respect to x^1 and Γ_{jk}^i are the Christoffel symbols of $\bar{g}$.

One can further simplify this expression by choosing the axes x^2 and x^3 such that x^2 aligns with the gradient of $\bar{g}_{11}$, which implies that $\Gamma_{13}^1 = \frac{1}{2}\partial_3 \bar{g}_{11} = 0$ on $\mathcal{S}$. Recalling that $E_{\lim}$ is the limit as $r \to 0$ of the elastic energy E_r divided by r^4, we can rewrite (2) as

$$E = \frac{Y\pi r^4}{8} \int_{\mathcal{S}} [(\kappa_2 - \bar{\kappa})^2 + \kappa_3^2 + (\tau - \bar{\tau})^2]dx^1 + O(r^6),$$

$$\tag{3}$$

where

$$\kappa_2 = \mathbf{q}_2' \cdot \mathbf{q}_1, \qquad \kappa_3 = \mathbf{q}_3' \cdot \mathbf{q}_1, \qquad \tau = \mathbf{q}_2' \cdot \mathbf{q}_3, \tag{4}$$

and

$$\bar{\kappa} = \Gamma_{12}^1 = \tfrac{1}{2}\partial_2 \bar{g}_{11}, \qquad \bar{\tau} = \Gamma_{13}^2 = \tfrac{1}{2}(\partial_2 \bar{g}_{13} - \partial_3 \bar{g}_{12}), \tag{5}$$

where the right-hand sides are evaluated on $\mathcal{S}$. Equation (5) shows how the spontaneous curvature $\bar{\kappa}$ and the spontaneous twist $\bar{\tau}$ emerge from the 3D intrinsic metric of the rod. Expression (3) coincides with the classical expressions for the energy of a rod in the cases of a Euclidean rod subject to bending and torsion but no stretching (e.g., [14]).

Equilibrium configuration.—In order for the $O(r^4)$ energy contribution in (3) to vanish, the following three conditions need to hold:

$$\kappa_2 = \bar{\kappa}, \qquad \kappa_3 = 0, \qquad \tau = \bar{\tau}. \tag{6}$$

Applying (6) and using the fact that $\mathbf{q} \in SO(3)$, we rewrite (4) as

$$\begin{pmatrix} \mathbf{q}_1 \\ \mathbf{q}_2 \\ \mathbf{q}_3 \end{pmatrix}' = \begin{pmatrix} 0 & \bar{\kappa} & 0 \\ -\bar{\kappa} & 0 & \bar{\tau} \\ 0 & -\bar{\tau} & 0 \end{pmatrix} \begin{pmatrix} \mathbf{q}_1 \\ \mathbf{q}_2 \\ \mathbf{q}_3 \end{pmatrix}. \tag{7}$$

Under free boundary conditions, Eq. (7) has a unique solution (modulo solid body transformations), obtained by identifying $\mathbf{q}$ with the Frenet-Serret triad (tangent, normal, and binormal unit vectors) of a curve whose curvature and torsion are $\bar{\kappa}$ and $\bar{\tau}$, respectively. Therefore, there is a unique midcurve configuration whose energy scales like $O(r^6)$, and it will hence be the limiting configuration for thin rods, regardless of the exact form of the higher-order terms.

Moreover, the limiting equilibrium configuration can be directly linked through (5) to the derivatives of the 3D intrinsic metric. We have therefore obtained a recipe for calculating the equilibrium configuration of an unconstrained thin rod from its intrinsic geometry.

We now make another important observation: In general, dimensionally reduced energy functionals emerge from specific three-dimensional energy functionals and are therefore model-dependent. On the other hand, the energy minimizing configuration for non-Euclidean rods imposes zero strain and zero strain derivatives on the midcurve. It follows that the equilibrium configuration found above remains the only $O(r^6)$ configuration under *any* reasonable elastic model, including Poisson ratio
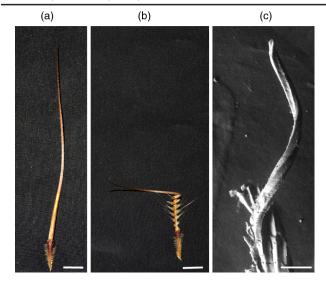
(a)   (b)   (c)

FIG. 1 (color online).   Thin elastic bodies in stork's bill. A
(a) wet and (b) dry awn (scale bar—1 cm). (c) Scanning electron
microscopy image of a dry cell taken from the top of the coiling
region of the awn (scale bar—50 μm).

(a)   (b)   (c)

FIG. 2 (color online).   (a) At every point on the cell wall, we
define the angle ψ between the orientation of the fibrils and the
cell's longitudinal axis. ψ is approximately independent of the
longitudinal coordinate x^1 but may depend on the azimuthal
direction χ within the cross section plane. (b) A regular helix, in
which $\psi(\chi)$ is constant and equals θ. (c) A tilted helix at tilt
angle ϕ, in which $\psi(\chi)$ ranges between $(\theta - \phi)$ and $(\theta + \phi)$,
where θ is the mean fibril angle.

effects, nonisotropic elastic moduli, and nonlinear re-
sponse. In this sense, the theory is much more robust for
the case of non-Euclidean rods than it is for the case of
non-Euclidean plates or shells.

Applications.—Stork's bill (*Erodium gruinum*) is a small
wild plant from the *Geraniaceae* family. This family is
characterized by beaklike fruits that break into five dis-
persal units at maturity. Each unit is equipped with a long
thin attachment, the awn, which demonstrates hygroscopic
movement. The awns of the stork's bill contract and form
helices [Fig. 1(a)]. We showed in [9] that the hygroscopi-
cally active tissue is constructed of long and thin cylindri-
cal cells, with lignified thick secondary cell walls. Each
cell in this tissue spirals spontaneously while it dries, and
adjacent cells interact to spiral cooperatively. The mecha-
nism is based on hygroscopic contraction in a sheared
helical arrangement of the cell wall cellulose microfibrils.
Upon dehydration, the matrix between the microfibrils
undergoes active contraction by some factor α in the
directions normal to the fibrils. Measurements show that
α is monotonic with humidity and typically varies in the
range 1 down to 0.5 [15].

Fibril orientations in the cell wall [Fig. 2(a)] are esti-
mated using small-angle x-ray scattering (SAXS) measure-
ments of the straight (wet) cells (see materials and methods
in [16]). The data indicate that the fibrils form a tilted helix,
and we denote by ϕ the tilt angle and by θ the mean fibril
angle [Figs. 2(b) and 2(c)]. These parameters reflect struc-
tural attributes of the cell that are independent of α and
remain fixed during dehydration.

Consider a material element on the cell wall at the
location $(x^1, r\cos\chi, r\sin\chi)$, where r is the radius of the
cell. When dried, this element maintains its length in
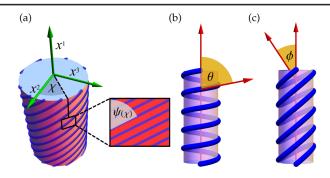the direction $\psi(\chi)$ of the fibrils but shrinks by a factor α

in the directions normal to the fibrils. In a local coordinate
system aligned with the fibrils, the reference metric of the
dried cell at the wall is

$$\bar{g}_{\text{local}} = \begin{pmatrix} 1 & 0 & 0 \\ 0 & \alpha^2 & 0 \\ 0 & 0 & \alpha^2 \end{pmatrix}.$$

To express this metric in a global Cartesian coordinate
system, we rotate $\bar{g}_{\text{local}}$ locally by an angle $\psi(\chi)$ about
the x^2 axis and then by an angle χ about the x^1 axis. We
thus get the three-dimensional metric on the cell wall

$$\bar{g}|_{(x^1, r\cos\chi, r\sin\chi)} = \mathcal{R}_1(\chi)\mathcal{R}_2[\psi(\chi)]\bar{g}_{\text{local}}$$
$$\times \mathcal{R}_2^{-1}[\psi(\chi)]\mathcal{R}_1^{-1}(\chi), \qquad (8)$$

where $\mathcal{R}_k(\psi)$ represents the rotation matrix by an angle ψ
around the k direction. For notational succinctness, we
denote $\bar{g}|_{(x^1, r\cos\chi, r\sin\chi)} = \bar{g}(r, \chi)$.

We approximate the first derivatives of $\bar{g}$ on the mid-
curve by the finite difference of its values at antipodal
points at the wall:

$$\partial_2\bar{g} \approx \frac{\bar{g}(r, 0) - \bar{g}(r, \pi)}{2r}$$
$$= -\frac{1-\alpha^2}{2r}\sin2\theta \begin{pmatrix} \sin2\phi & 0 & -\cos2\phi \\ 0 & 0 & 0 \\ -\cos2\phi & 0 & -\sin2\phi \end{pmatrix},$$

$$\partial_3\bar{g} \approx \frac{\bar{g}(r, \pi/2) - \bar{g}(r, 3\pi/2)}{2r}$$
$$= -\frac{1-\alpha^2}{2r}\sin2\theta \begin{pmatrix} 0 & 1 & 0 \\ 1 & 0 & 0 \\ 0 & 0 & 0 \end{pmatrix}.$$

These expressions need further refinement. It is explicitly
assumed in the derivation of (2) that $\bar{g}$ on the midcurve is

the unit tensor. Averaging $\bar{g}(r, \chi)$ over all angles, χ shows that $\langle \bar{g}_{11} \rangle = \cos^2\theta + \alpha^2 \sin^2\theta$. We thus reparametrize the x^1 axis by a multiplicative factor of $\sqrt{\langle \bar{g}_{11} \rangle}$. By (5), the intrinsic curvature and torsion of the cell is

$$\bar{\kappa} \approx -\tfrac{1}{2}\partial_2 \bar{g}_{11} = c(\alpha, \theta)\sin 2\phi,$$
$$\bar{\tau} \approx \tfrac{1}{2}(\partial_2 \bar{g}_{13} - \partial_3 \bar{g}_{12}) = c(\alpha, \theta)(1 + \cos 2\phi), \tag{9}$$

where

$$c(\alpha, \theta) = \frac{(1 - \alpha^2)\sin 2\theta}{4r\sqrt{\cos^2\theta + \alpha^2 \sin^2\theta}}.$$

As explained, the equilibrium configuration of the rod is a curve whose curvature and torsion are $\bar{\kappa}$ and $\bar{\tau}$, respectively. Since $\bar{\kappa}$ and $\bar{\tau}$ are independent of x^1, the resulting curve is a helix, characterized by

$$\text{pitch} = \frac{2\pi\bar{\tau}}{\bar{\kappa}^2 + \bar{\tau}^2} = \frac{\pi}{c(\alpha, \theta)},$$
$$\text{pitch angle} = \tan^{-1}(\bar{\tau}/\bar{\kappa}) = \frac{\pi}{2} - \phi. \tag{10}$$

Note that we now have two different helical structures: a tilted helix that describes the microscopic structure of the cell and a straight helix that describes the cell's macroscopic configuration.

The model predictions are summarized in Fig. 3. For $\phi = 0$, (9) and (10) predict an equilibrium configuration which is unbent, i.e., a purely twisted rod, as expected from the azimuthal symmetry of the rod structure. This is in agreement with our measurements of cranesbill cells (Table I) and with the results of [17] in the study of spruce
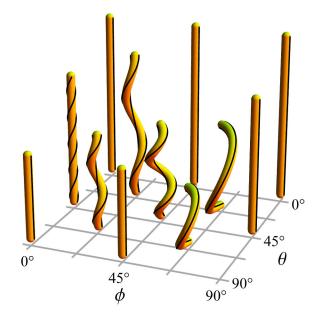

FIG. 3 (color online). Predicted shapes for different cells with several values of the cell parameters θ and ϕ, for $\alpha = 0.5$. The black lines on the sides of each rod represent the $\pm x^2$ directions in intrinsic coordinates.

cells. In the moist case, $\alpha = 1$, all cells fulfill $c(\alpha, \theta) = 0$ and therefore their curvature and torsion both vanish.

Notice that the pitch angle depends neither on the shrinkage ratio α, nor on the mean angle of the fibrils θ, nor on the radius of the cell r. This implies that, modulo an isotropic rescaling, the equilibrium configuration of the cell depends only on the tilt parameter ϕ. This fact is demonstrated in Figs. 4(a) and 4(b), where we superimpose rescaled images of a cell at different stages of drying (see the method in [16]) onto one another.

In the process of drying, the conformational changes are entirely due to the decrease in the shrinkage ratio α (from an initial "moist" value of 1). The structural parameters θ, ϕ, and r are expected to remain constant. To estimate these parameters from the shape of the cell, we measure the pitch and the total length of the cell and solve an algebraic system of equations for α and θ, while ϕ can be inferred directly from the pitch angle using (10). In all measured cell types, while α decreases by 25%–50% during dehydration, both θ and ϕ vary only by a few percents, as expected from the model.

We use this method to calculate θ and ϕ for stork's bill cells from the bottom (B) and top (T) inner parts of the coiling region, as well as for cells from the awn of cranesbill (*Geranium pusillum*). The results are consistent with the independent SAXS measurements (Table I).

To conclude, we developed a dimensionally reduced 1D model for thin non-Euclidean elastic rods. In particular, we derived a recipe for calculating the spontaneous twist and curvature, as well as the equilibrium configuration, of a thin elastic rod from its internal 3D structure. This robust method is applicable to a wide variety of elastic models. The model was applied to the study of stork's bill and cranesbill cells and their configurational response to dehydration. We have quantitatively shown that the recently discovered helical shape of the dried cells results from the arrangement of cellulose fibrils in their walls.

The entire awn of the common stork's bill attains a coiling configuration when dried. Mechanically, the awn is nothing more than an aggregate of cells; each follows the physics of thin rods we described in this Letter. Further work should therefore be done in order to connect the collective behavior of the sheaf with the internal geometry of each single rod.

TABLE I. θ and ϕ for different cell types, as calculated from the cell's conformational changes during dehydration and as measured by SAXS.

Cell	θ		ϕ	
	Shape	SAXS	Shape	SAXS
Stork's bill (B)	$69°(\pm 5°)$	$\geq 65°$	$28°(\pm 5°)°$	$20°(\pm 5°)$
Stork's bill (T)	$82°(\pm 5°)$	$\geq 65°$	$15°(\pm 5°)°$	$10°(\pm 5°)$
Cranesbill	$5°(\pm 8°)$	$\leq 20°$	$0°(\pm 5°)°$	$0°(\pm 5°)$

(a)   (b)

FIG. 4 (color online).   (a) Raw images of a cell at different shrinkage ratios α (scale bar—100 μm). (b) The same images isotropically rescaled and superimposed onto one another to demonstrate collapse onto the same curve. Calculation of the internal structure parameters from these shapes shows a decrease in α from 1 to $\sim$0.7, with approximately constant $\theta = 69° \pm 5°$ and $\phi = 28° \pm 5°$.

[1] E. Reyssat and L. Mahadevan, J. R. Soc. Interface **6**, 951 (2009).
[2] S. Armon, E. Efrati, E. Sharon, and R. Kupferman, Science **333**, 1726 (2011).
[3] R. Elbaum, L. Zaltzman, I. Burgert, and P. Fratzl, Science **316**, 884 (2007).
[4] J. Yin, Z. Cao, C. Li, I. Sheinman, and X. Chen, Proc. Natl. Acad. Sci. U.S.A. **105**, 19 132 (2008).
[5] H. Liang and L. Mahadevan, Proc. Natl. Acad. Sci. U.S.A. **106**, 22 049 (2009).
[6] A. Goriely and M. Ben Amar, Phys. Rev. Lett. **94**, 198103 (2005).
[7] Y. Forterre, J. Skotheim, J. Dumais, and L. Mahadevan, Nature (London) **433**, 421 (2005).
[8] A. Goriely and M. Tabor, Phys. Rev. Lett. **80**, 1564 (1998).
[9] Y. Abraham, C. Tamburu, E. Klein, J. Dunlop, P. Fratzl, U. Raviv, and R. Elbaum, J. R. Soc. Interface **9**, 640 (2011).
[10] C. W. Wolgemuth, Y. F. Inclan, J. Quan, S. Mukherjee, G. Oster, and M. A. R. Koehl, Phys. Biol. **2**, 189 (2005).
[11] A. Goriely and M. Tabor, Nonlinear Dynamics **21**, 101 (2000).
[12] R. Kupferman and J. Solomon, "A Riemannian approach to reduced plate, shell, and rod theories" (to be published).
[13] G. Friesecke, R. James, and S. Müller, Commun. Pure Appl. Math. **55**, 1461 (2002).
[14] L. Landau and E. Lifshitz, *Theory of Elasticity* (Pergamon, New York, 1959).
[15] C. Kennedy, A. Šturcová, M. Jarvis, and T. Wess, Cellulose **14**, 401 (2007).
[16] See Supplemental Material at http://link.aps.org/supplemental/10.1103/PhysRevLett.108.238106 for experimental materials and methods.
[17] I. Burgert, K. Fruhmann, J. Keckes, P. Fratzl, and S. Stanzl-Tschegg, Holzforschung **59**, 247 (2005).